Journal of Operation and Automation in Power Engineering

vol. 13, no. Special Issue, Dec. 2025, Pages: 62-74

http://joape.uma.ac.ir

Research Paper

A Multi-Objective Optimization Method for the Best Concurrent Involvement of Energy Networks and Energy Hubs

Javohir Zokirov [1, *], *Dilafruz Kholmurodova* [2], *Akmal Rustamov* [3], *Rovshan Khakimov* [4], *Ilkhom Rasulov* [5], *Yusuf Turdibekov* [6], *Sardorbek Yusufov* [7], and *Fazliddin Jumaniyazov* [8]

[1]*Termiz University of Economics and Service, Farovon Street 4-b, Termez, Surxondaryo, Uzbekistan.*
[2]*Scientific and Practical Center of Immunology, Allergology and Human Genomics, Samarkand State Medical University, Samarkand, Uzbekistan.*
[3]*Kimyo International University in Tashkent, Tashkent, Uzbekistan.*
[4]*Tashkent State Transport University, 100167 Tashkent, Uzbekistan.*
[5]*Department of Russian Language and Literature, Kokand State University, Kokand, Uzbekistan.*
[6]*Samarkand State University of Architecture and Civil Engineering, Samarkand, Uzbekistan.*
[7]*Department of "Architecture", Urgench State University, Urgench, Uzbekistan.*
[8]*Mamun University, 220912 Khiva, Khorezm, Uzbekistan.*

Abstract— *In this study a framework for the best possible simultaneous involvement of energy systems and energy hubs in day-ahead energy shops is presented. The suggested method is a multi-objective optimization problem and takes into account both wholesale and retail market structures. The primary objective function seeks to reduce the overall energy costs of thermal, gas, and electricity networks. By optimizing the difference between energy purchase and sales costs, the second goal function aims to reduce the energy costs of energy hubs in the retail market. The operational model of active resources and loads inside the energy hubs, as well as the optimal power flow calculations of the integrated energy systems, place limitations on the suggested model. To solve the optimization problem, a Pareto-based weighted sum method combined with fuzzy decision-making is employed to derive a compromise optimal solution. Finally, the proposed framework is implemented on a test system, and the numerical results confirm its effectiveness in successful economic performance of energy hubs and simultaneously enhancing the cost-effective and operational conditions of integrated energy networks which reduce energy cost up to a ∼40%.*

Keywords—Energy hubs, integrated energy networks, day-ahead energy markets, multi-objective optimization.

1. INTRODUCTION

The increasing deployment of electric vehicles (EVs), combined heat and power (CHP) units, and renewable energy sources (RESs) has substantially improved the flexibility and efficiency of modern multi-carrier energy systems. Demand response programs (DRPs) further enhance sustainability by shaping more efficient consumption behavior. While these active resources and loads (ALs) offer considerable operational and economic advantages [1], their widespread integration across electrical, gas, and thermal infrastructures also increases system complexity [2]. The resulting surge in operational data and interdependencies imposes significant challenges on energy network operators (ENOs), who require advanced optimization tools to maintain reliable and efficient system performance [3, 4].

Received: 27 Nov. 2025
Revised: 23 Dec. 2025
Accepted: 25 Dec. 2025
*Corresponding author:
E-mail: javohir_zokirov@tues.uz (Z. Javohir)
DOI: 10.22098/joape.2025.18918.2469

Emerging renewable technologies—such as piezoelectric energy harvesting and flow-induced vibration–based power generation [5]—further highlight the importance of integrated multi-carrier energy management frameworks like the one proposed in this study, as their dynamic and distributed nature requires coordinated scheduling across electrical, thermal, and gas networks [6]. The smart grid framework enables coordinated management of active resources and loads (ALs) through aggregators such as virtual power plants (VPPs) [7], microgrids (MGs), and energy hubs (EHs), with EHs offering the unique ability to control multiple energy carriers simultaneously [8]. In integrated energy networks (ENs), the interaction between ALs, EH operators, and energy network operators (ENOs) establishes a multi-directional coordination structure that enhances operational flexibility and economic performance [9]. Prior research has proposed various optimization strategies for EHs within ENs. For instance, the model in [10] introduced a robust, computationally efficient EH optimization framework using linearized OPF and gas-flow approximations, demonstrating minimal accuracy loss and improved system efficiency [11].

Various optimization techniques have become essential tools across diverse engineering disciplines, enabling the systematic design [12], analysis, and control of complex systems under multi-domain operational constraints [13]. This section expands on previous studies regarding the operation and optimization of EHs within integrated energy networks [14]. In [15], an

EH incorporating renewable energy sources (RESs), demand response courses, and energy storage structures was analyzed. The study evaluated the impact of storage systems on EH operation, demonstrating that energy storage reduces peak demand by storage energy throughout off-peak hours and discharging it throughout highest periods. In [16], a robust operational model for EHs joined to both electrical and gas microgrids was developed, incorporating adaptive robust optimization to account for uncertainties in RES generation and demand. The problem was formulated as a Min-Max-Min optimization model, which was solved using Benders decomposition. The method consisted of a master problem, which addressed unit commitment, and a subproblem, which optimized microgrid operation with EHs. In [17], a stochastic operation model for microgrids including EHs with photovoltaic panels and compressed air storage was proposed. The study showed that the optimized operation of EHs effectively reduced energy losses and operational charges within microgrids. In [18], an environmentally constrained optimal EH operation model was introduced, demonstrating that RESs, such as solar panels and wind turbines, enhance operational efficiency and contribute to clean energy supply. Ref. [19] examined the reliability improvement potential of EHs under N-1 contingencies. The results indicated that EHs, due to their proximity to demand centers, significantly reduce outages, thereby enhancing system reliability.

Various studies have investigated the participation of EHs in energy markets [20]. Ref. [21] explored the role of EHs in electricity markets under bilateral contracts and power pooling models. While [22] presented a deterministic model, [23] employed a robust optimization approach to address uncertainties in electricity prices, demand, and RES generation. The findings demonstrated that EHs can secure financial benefits through optimal resource scheduling even under worst-case uncertainty scenarios. Ref. [24] extended the analysis to EH participation in electricity, gas, and thermal energy markets, highlighting that EHs generally act as gas consumers due to their reliance on CHP systems and boilers while serving as electricity and thermal energy producers, thereby generating revenue in these markets. In [25], energy pricing was treated as a variable derived from the market-clearing price rather than a fixed parameter, allowing for a more dynamic market representation.

Ref. [26] introduced stochastic dynamic programming (SDP) for optimal EH operation, while [27] analyzed EH operation under network reliability and flexibility constraints in electrical, thermal, and gas networks. Expected unserved energy (EUE) was used to assess reliability, and an energy flexibility index was introduced to quantify operational adaptability. Ref. [28] applied adaptive robust optimization to model uncertainties in demand, RES generation, and energy prices for EH operation across multiple networks. Finally, [29] focused on residential-scale EH operation, considering the integration of EVs and evaluating their capabilities within EH frameworks. Ref. [30] examines the integration of EHs with EVs and hydrogen storage systems. A hybrid stochastic-robust model is employed to address uncertainties in demand, renewable energy generation, and EV aggregation parameters. A review of the literature indicates that most studies focus on EH operation, while fewer address their participation in energy markets. Additionally, existing market models for EHs often do not incorporate energy network interactions, treating EHs in isolation. However, in a competitive market environment, where financial benefits for participants and social welfare improvements are key objectives, it is crucial to evaluate the joint operation of distribution companies (DisCos) and EHs in energy markets. Despite extensive research on energy hub (EH) operation and multi-energy optimization, several key gaps remain unresolved. First, most existing EH models focus on internal scheduling and do not fully capture market-interactive operation, where EHs actively participate in retail and wholesale transactions and strategically inject or purchase multi-carrier energy based on price signals. Second, the literature seldom addresses joint optimization between distribution companies (DisCos) and EHs. Prior studies commonly optimize these entities separately or impose unidirectional interactions, overlooking the bidirectional operational and economic interdependencies that arise when EHs serve simultaneously as flexible loads and distributed producers. Third, multi-carrier interaction in retail markets remains insufficiently modeled: energy prices and flows for electricity, gas, and thermal carriers are often treated independently, neglecting cross-carrier substitution, conversion, and coupling effects that fundamentally influence both operational feasibility and economic outcomes. These gaps demonstrate the need for a unified optimization framework that co-optimizes DisCo and EH decisions, explicitly models cross-carrier interactions, and incorporates market participation mechanisms—motivating the methodology proposed in this study.

Although numerous studies have examined optimal EH operation and multi-energy OPF formulations, several methodological gaps remain unaddressed. First, most EH-focused works optimize internal operation while assuming fixed or simplified interactions with upstream energy networks, thereby overlooking the bidirectional coupling and market-driven exchange that occur in real systems. Second, EN-level optimization studies typically treat EHs as inflexible demand components, ignoring their ability to inject power, heat, or gas into multiple networks and participate strategically in multi-energy markets. Third, a large portion of the literature relies on sequential or loosely coordinated decision structures, which fail to capture the simultaneous technical and economic interdependencies between EHs and ENs. Finally, existing multi-objective frameworks seldom incorporate a unified compromise-selection mechanism capable of supporting coordinated market participation under conflicting objectives. These limitations collectively justify the need for the integrated multi-objective optimization and fuzzy decision-making framework proposed in this study, which explicitly models EH–EN coupling and supports concurrent operational and economic decision-making across multiple carriers. To bridge this gap, the research proposes a comprehensive and retail energy market model for several energy systems, including thermal, gas, and electrical systems, in the existence of EHs. The model effectively distributes energy resources and active loads while taking into account the coordination between EH operators and energy network operators. In this framework, private distribution companies participate in wholesale markets to purchase energy, which is then redistributed in retail markets among connected consumers. In order to minimize the weighted total of energy costs for DisCos in extensive and retail markets as well as EH energy costs in retail marketplaces, the suggested model is constructed as a bi-objective optimization problem. The optimization problem is limited by the operational restrictions of EH resources and active loads, as well as optimal power flow (OPF) formulae for various networks. To find a compromise solution, a fuzzy decision-making method based on Pareto is used.

Although multi-energy OPF, EH modeling, and fuzzy decision-making have been individually addressed in prior research, the present study introduces a unified methodological framework that enables the concurrent optimization of energy networks and interconnected energy hubs. The proposed approach advances the state of the art through:

1) A mathematically integrated multi-objective structure that treats networks and hubs as co-optimized subsystems rather than sequential or decoupled entities;
2) An enhanced representation of inter-carrier coupling enabling simultaneous decisions across electricity, gas, and heat domains;
3) A generalized fuzzy decision-making mechanism specifically adapted to multi-energy operational objectives, improving the interpretability and robustness of Pareto-front compromise solutions;
4) A scalable OPF–EH coordination model that reduces

computational complexity while retaining high-fidelity operational constraints.

These contributions collectively distinguish the proposed method from existing multi-energy optimization techniques and establish its novelty.

2. Optimization Model for Energy Networks in the Presence of Energy Hubs

This section formulates the optimal operation of ENs in the presence of EHs, considering their participation in the energy market. The objective function aims to minimize the subjective sum of the energy costs of various networks and EHs while satisfying the constraints related to optimal power flow and the operation of active resources and loads within EHs. The formulation of this model is as follows:

$$\min\ CF = \nu_1 \mathrm{Cost}_{ENs} + \nu_2 \mathrm{Cost}_{EHs} \tag{1}$$

$$\mathrm{Cost}_{ENs} = \sum_t \left(\lambda_t^{wh} P_t^{wh} + \sum_k \lambda_t^{ret} P_{k,t}^{EH \to EN} \right) \tag{2}$$

$$\mathrm{Cost}_{EHs} = \sum_{k,t} \left(\lambda_t^{ret} P_{k,t}^{EN \to EH} - \lambda_t^{ret} P_{k,t}^{EH \to EN} \right) \tag{3}$$

$$P_{i,t}^{gen} - P_{i,t}^{load} + P_{i,t}^{EH} = \sum_{j \in \Omega_i} P_{ij,t} \tag{4}$$

$$Q_{i,t}^{gen} - Q_{i,t}^{load} + Q_{i,t}^{EH} = \sum_{j \in \Omega_i} Q_{ij,t} \tag{5}$$

$$P_{ij,t} = V_{i,t} V_{j,t} (G_{ij} \cos\theta_{ij,t} + B_{ij} \sin\theta_{ij,t}) \tag{6}$$

$$Q_{ij,t} = V_{i,t} V_{j,t} (G_{ij} \sin\theta_{ij,t} - B_{ij} \cos\theta_{ij,t}) \tag{7}$$

$$V_i^{\min} \le V_{i,t} \le V_i^{\max} \tag{8}$$

$$P_{ij,t}^2 + Q_{ij,t}^2 \le S_{ij}^{\max 2} \tag{9}$$

$$\sum_{j \in \Omega_i} F_{ij,t}^g + F_{i,t}^{EH,g} = F_{i,t}^{load,g} \tag{10}$$

$$p_{i,t}^2 - p_{j,t}^2 = K_{ij} (F_{ij,t}^g)^2 \tag{11}$$

$$p_i^{\min} \le p_{i,t} \le p_i^{\max} \tag{12}$$

$$\sum_{j \in \Omega_i} Q_{ij,t}^h + Q_{i,t}^{EH,h} = Q_{i,t}^{load,h} \tag{13}$$

$$Q_{ij,t}^h = Q_{ij,t}^{send} - \lambda_{ij}^h (T_{ij,t} - T_{amb}) \tag{14}$$

$$T_i^{\min} \le T_{i,t} \le T_i^{\max} \tag{15}$$

$$P_{k,t}^{in,e} - P_{k,t}^{out,e} + \eta_e^{CHP} P_{k,t}^{CHP} - P_{k,t}^{load,e} = 0 \tag{16}$$

$$F_{k,t}^{in,g} - F_{k,t}^{out,g} - F_{k,t}^{CHP} - F_{k,t}^{Boiler} = 0 \tag{17}$$

$$Q_{k,t}^{in,h} - Q_{k,t}^{out,h} + \eta_h^{CHP} F_{k,t}^{CHP} + \eta^{Boiler} F_{k,t}^{Boiler} = Q_{k,t}^{load,h} \tag{18}$$

$$P_{k,t}^{CHP} = \eta_e^{CHP} F_{k,t}^{CHP} \tag{19}$$

$$\tau = 1 - \frac{\sum_{i=1}^{N_{gen}} \lambda_i P_i}{\sum_{i=1}^{N_{gen}} P_i} \tag{20}$$

$$Q_{k,t}^{Boiler} = \eta^{Boiler} F_{k,t}^{Boiler} \tag{21}$$

$$E_{k,t} = E_{k,t-1} + \eta^{ch} P_{k,t}^{ch} - \tfrac{1}{\eta^{dis}} P_{k,t}^{dis} \tag{22}$$

$$E_k^{\min} \le E_{k,t} \le E_k^{\max} \tag{23}$$

$$0 \le P_{k,t}^{ch} \le P_k^{ch,\max} \tag{24}$$

$$0 \le P_{k,t}^{dis} \le P_k^{dis,\max} \tag{25}$$

$$E_{k,t}^{EV} = E_{k,t_0}^{EV} \text{ if EV absent at time } t \tag{26}$$

$$-v_i P_{i,t}^D \le P_{i,t}^{DR} \le v_i P_{i,t}^D \tag{27}$$

$$-v_i Q_{i,t}^D \le Q_{i,t}^{DR} \le v_i Q_{i,t}^D \tag{28}$$

$$-v_i F_{i,t}^D \le F_{i,t}^{DR} \le v_i F_{i,t}^D \tag{29}$$

$$\sum_t P_{i,t}^{DR} = 0 \tag{30}$$

$$\sqrt{(P_{k,t}^{dis})^2 + (Q_{k,t})^2} \le S_k^{\max} \tag{31}$$

$$\sqrt{P_{E,t}^2 + Q_{E,t}^2} \le \bar{S}_E \tag{32}$$

$$Q_{i,t}^2 + P_{i,t}^2 \leq \bar{S}_i^2 \tag{33}$$

$$\sqrt{P_{R,t}^2 + Q_{R,t}^2} \leq \bar{S}_R \tag{34}$$

$$-v_i P_{i,t}^D \leq P_{i,t}^{DR} \leq v_i P_{i,t}^D \tag{35}$$

$$-v_i P_{i,t}^{market} \leq P_{i,t}^{DR} \leq v_i P_{i,t}^{market} \tag{36}$$

$$\sum_{t \in \Pi_{OB}} P_{i,t}^{DR} = 0 \tag{37}$$

$$\begin{aligned} &P_{EH,i,t}^{+} - P_{EH,i,t}^{-} = P_{C,i,t} + P_{R,i,t} + P_{DR,i,t} + \\ &P_{DIS,i,t} - P_{CH,i,t} - P_{D,i,t}, \quad \forall i,t \\ &P_{EH,i,t}^{+} \geq 0, \quad P_{EH,i,t}^{-} \geq 0, \quad \forall i,t \end{aligned} \tag{38}$$

For clarity and readability, all symbols, parameters, and decision variables used in Eqs. (1)-(37) are defined in Table 1.

Table 1. Nomenclature symbols, and parameters.

Symbol	Description	Unit
h	Time index (hour), (h = 1,...,24)	–
i	Bus index	–
k	Electric vehicle (EV) index	–
ΩDG	Set of distributed generation units	–
ΩPV	Set of photovoltaic units	–
ΩEV	Set of electric vehicles	–
$P_{grid}(h)$	Power purchased from upstream grid at hour (h)	kW
$PDG,i(h)$	Active power output of DG unit (i)	kW
$PPV,i(h)$	Active power output of PV unit (i)	kW
$Pkch(h)$	Charging power of EV (k)	kW
$Pkdis(h)$	Discharging power of EV (k)	kW
$Ek(h)$	Energy stored in EV battery	kWh
$\Delta PDR(h)$	Demand response load shift	kW
$\rho(h)$	Electricity price at hour (h)	$/kWh
$Ctotal(h)$	Total operating cost	$
Ai, Bi, Ci	DG cost coefficients	–
$PDG,imin,\ PDG,imax$	DG output limits	kW
$PPV,imax(h)$	Available PV power	kW
EV	charging/discharging limits	kW
$Ekmin,\ Ekmax$	EV battery energy limits	kWh
$Ekreq$	Required EV energy at departure	kWh
$\eta ch,\ \eta dis$	Charging/discharging efficiency	–
Δt	Time step duration	h
$Vi(h)$	Voltage magnitude at bus (i)	p.u.
$Vmin, Vmax$	Voltage limits	p.u.
$Ploss(h)$	Network active power loss	kW

The objective function of the problem is presented in Eq. (1), which includes the weighted sum of the energy costs of electrical, gas, and thermal systems in extensive and retail markets (Cost_{ENs}) and energy price of EHs in retail market (Cost_{EHs}). The contribution perfect of EHs and ENs in energy marketplace is schematically illustrated in Fig. 1. Accordingly, ENs procurements energy from the extensive market and distribute it among customers and EHs in the retail market. Given that EHs consume energy generation and storing components, their energy management allows them to act as producers. Therefore, EHs can wholesale energy to ENs in retail market. Based on this framework, the cost of ENs includes the cost of purchasing energy from the wholesale market (first term) and the cost of purchasing energy from EHs in the retail market (second term). The second term serves as an incentive mechanism for EHs. Eq. (3) formulates the energy cost of EHs (Cost_{EHs}), which, based on Fig. 1 and the provided explanations, refers to change between the energy obtained by EHs and the energy they sell in retail market.

The restraints related to energy systems are presented in Eqs. (4) to (24). Eqs. (4) to (7) correspond to AC power flow model in the electrical network, including active and reactive power equilibrium equations at electrical cars and power flow equations for distribution lines. Additionally, the constraints related to gas system power flow are given in Eqs. (8) and (9), which describe the power balance at gas nodes and the power flow through gas pipelines. Similarly, power flow model in thermal system is formulated in Eqs. (10) and (11).

The operational constraints of electrical, gas, and thermal networks are modeled in Eqs. (12) to (14), (15) to (17), and (18) to (20), respectively. These constraints include the voltage limits of electrical buses, the ostensible power limits of supply lines and substations, the pressure limits of gas nodes, and the temperature constraints of thermal nodes and pipelines.

The operation model of active resources and loads, including storage units and responsive loads, is presented in Eqs. (21) to (37). This model considers the balance constraints of active, reactive, thermal, and gas power in EHs. Additionally, the operational models of combined heat and power (CHP) systems, boilers, and energy storage units are provided in this section. Among these, the operation model of electrical energy storage units and EVs is expressed in Eqs. (31) to (34). It is noteworthy that the amount and kind of EVs joined to EHs at any given moment may vary, leading to dynamic changes in charging/discharging rates, storage capacity, and initial/final energy levels. In this study, it is expected that each EV fully controls its battery.

Finally, the models for renewable energy sources and demand response programs (DRPs) are presented in Eqs. (35) to (37). The DRP is designed based on an incentive-based model, where consumers adjust their energy consumption in response to price signals. This program shifts consumption from peak hours to off-peak hours, contributing to energy optimization. After defining the optimization model, the problem is solved using nonlinear programming solvers available in GAMS. Given the non-convexity introduced by AC power flow constraints, gas–thermal coupling, and multi-carrier conversion relations, multiple solvers—IPOPT, CONOPT, KNITRO, DISOPT, and OQNLP—were tested to evaluate robustness. IPOPT was selected as the reference solver due to its superior convergence behavior and computational efficiency across repeated trials. Solver settings such as tolerances, iteration limits, and initialization strategies are documented in this subsection. Evolutionary algorithms (GWO, SCA, KHO, CSA) are used only for validation and comparative benchmarking.

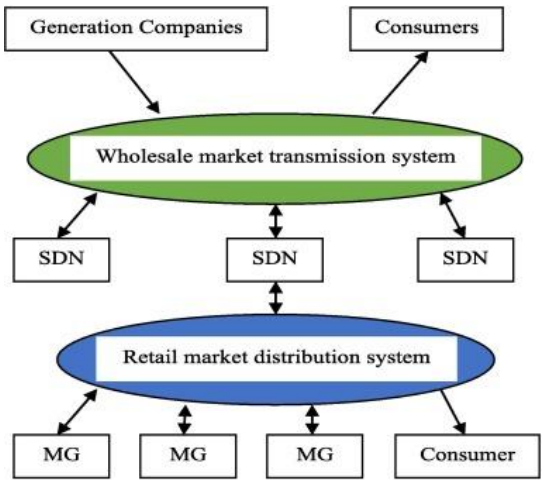

Fig. 1. Market participation framework of energy systems and energy centers in extensive and retail energy marketplaces [31].

3. Determination of Solution Established on Fuzzy Decision-Making

In Eq. (1), constraints v_1 and v_2 represent the weighting constants of the cost functions $\mathrm{Cost_{ENs}}$ and $\mathrm{Cost_{EHs}}$, respectively. Based on [32], their sum must be equivalent to 1. By selecting dissimilar values for these constraints, various trade-offs between $\mathrm{Cost_{ENs}}$ and $\mathrm{Cost_{EHs}}$ can be obtained, forming a Pareto front that represents the proposed framework. To determine an optimum compromise solution between these functions, fuzzy decision-making is employed [33].

In this approach, the optimization problem Eqs. (1)-(37) is solved for two extreme cases where $v_1 = 1$, $v_2 = 0$ and $v_1 = 0$, $v_2 = 1$. The results of these two cases yield the minimum (f_{min}) and maximum (f_{max}) values for the cost functions $\mathrm{Cost_{ENs}}$ and $\mathrm{Cost_{EHs}}$. Subsequently, for a given set of weighting constants, the membership function (f_l) is computed for $\mathrm{Cost_{ENs}}$ and $\mathrm{Cost_{EHs}}$. The membership function f_l for f is defined as 1 (0) if function value is fewer (greater) than its smallest (extreme) value. Otherwise, f_l is calculated as:

$$f_l = \frac{f - f_{max}}{f_{min} - f_{max}} \tag{39}$$

Next, the minimum $\mathrm{f_l}$ value obtained for $\mathrm{Cost_{ENs}}$ and $\mathrm{Cost_{EHs}}$ is determined, denoted by Δ. Lastly, the negotiation solution agrees to the point (with specific v_1 and v_2) that yields the maximum Δ. The stages of the fuzzy decision-making process are as:

1) Compute $\mathrm{f_{max}}$ and $\mathrm{f_{min}}$ for $\mathrm{Cost_{ENs}}$ and $\mathrm{Cost_{EHs}}$ by solving the problem for the two cases:
   - o $v_1 = 1$, $v_2 = 0$
   - o $v_1 = 0$, $v_2 = 1$
2) Compute $\mathrm{f_l}$ for the cost functions $\mathrm{Cost_{ENs}}$ and $\mathrm{Cost_{EHs}}$.
3) Determine Δ, where:
   $\Delta = \min\left(\mathrm{f_l}\left(\mathrm{Cost_{ENs}}\right)\right), \mathrm{f_l}\left(\mathrm{Cost_{EHs}}\right)$
4) Update the weighting coefficients as:
   $v_1 = v_1 - \varepsilon,\ v_2 = v_2 + \varepsilon$
   in which ε is a predefined step size (e.g., 0.05).
5) Repeat steps 2 and 3.
6) If $v_1 = 1$, proceed to step 7; otherwise, return to step 4.
7) Identify the cooperation answer conforming to the point with the maximum Δ.

Finally, the overall solution framework is illustrated in Fig. 2. The combined use of the weighted-sum method and fuzzy decision-making is motivated by the complementary strengths of these two techniques. The weighted-sum approach enables the generation of a continuous Pareto set by systematically varying the weighting coefficients, yet it does not provide a unique compromise solution and may yield ambiguous results in the presence of non-convex Pareto fronts. In contrast, fuzzy decision-making offers a rigorous mechanism for evaluating and ranking Pareto-optimal points by measuring their closeness to ideal objective values; however, it requires a predefined set of candidate solutions and does not independently generate the Pareto frontier. The hybrid approach adopted in this study leverages both capabilities: the weighted-sum method constructs a comprehensive Pareto front for the bi-objective optimization problem, and the fuzzy technique selects a final compromise solution that balances $\mathrm{Cost_{ENs}}$ and $\mathrm{Cost_{EHs}}$ in a mathematically transparent and robust manner.

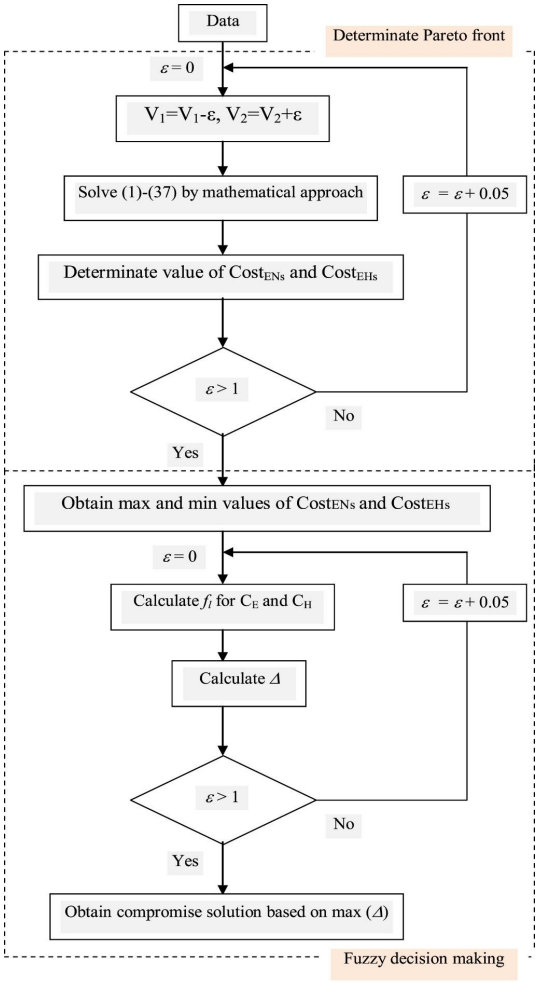

Fig. 2. Flowchart of the proposed optimization framework.

4. Statistics

In this segment, the suggested framework is applied to a benchmark test system, as illustrated in Fig. 3, which consists of a nine-bus electrical system, a four-node gas system, and a seven-node thermal system. The improper power in the electrical system is set to 1 MVA, while the base power in the gas and thermal networks is 1 MW. The base values for voltage, pressure, and temperature are 1 kV, 10 bar, and $100^{\circ}C$, respectively, with permissible variations within the range of [0.9, 1.1] per unit. The specifications of distribution lines, gas pipelines, and thermal connections are provided in [34]. The peak-load data for the thermal and electrical networks are also described in [34]. In gas system, CHP units and boilers are sole customers, with a passive gas load of zero. The hourly capacity data are determined by multiplying the highest load by the load influence, where the expected daily load factor curve for the electrical network is segmented into four time intervals: 00:01–07:00, 08:00–16:00, 17:00–22:00, and 23:00–24:00, with respective electricity prices of 17.6, 25.4, and 36 \$/MWh. The gas energy prices for intervals 00:01–04:00 (04:00–01:00), 16:00–24:00 (24:00–23:00), and 05:00–15:00 (22:00–05:00) are 22 and 30 \$/MWh, respectively [34]. It is supposed that ENs increase the retail market price by 25% over wholesale market price, i.e., $\lambda_{\mathrm{R}} \times \mathrm{W}$.

The network comprises seven energy hubs, the locations of which are specified in Figure 3, while their corresponding loads are provided in [34]. EHs 1–3 and 5 integrate various electrical assets, including Renewable Energy Sources (RES), EVs, batteries, and demand-responsive electrical loads. EH 4 is equipped with CHP units, boilers, and demand-responsive current loads. Hubs 6 and 7 encompass all aforementioned components. The CHP units have a extreme electrical and thermal production of 1.2 MVA and 2.3 MW, with efficiencies of $\eta_T = 40\%$, $\eta_L = 9\%$, and $\eta_H = 40\%$ [33]. The boiler operates with an efficiency of 80% and has a extreme thermal output of 0.3 MW. RES-equipped hubs integrate 0.25 MVA photovoltaic (PV) systems and 0.2 MVA wind turbines. The power generation of RES is determined by increasing its

volume by the generation rate, with the expected daily generation rate curves for PV and wind systems reported in [30].

Batteries, with a charge/discharge efficiency of 0.85 and a capacity of 3.2 MWh, are installed in EHs 1–3 and 5–7. These batteries feature a charge/discharge amount of 0.6 MW and a mount volume of 0.5 MVA. The smallest storable energy and first energy levels are both set to 0.3 MWh [14]. Each of EHs 1–3 and 5–7 can accommodate up to 60 EVs, with each EV characterized by charging/discharging rates, charger capacity, and other parameters specified in [35]. The whole amount of EVs in parking lot multiplied by EVs penetration rate determines how many EVs are connected to each EH at any given time. Fig. 4 shows the anticipated daily penetration rate curve for EVs. Hubs are projected to have a 30% participation rate in the Demand Response Program (DRP).

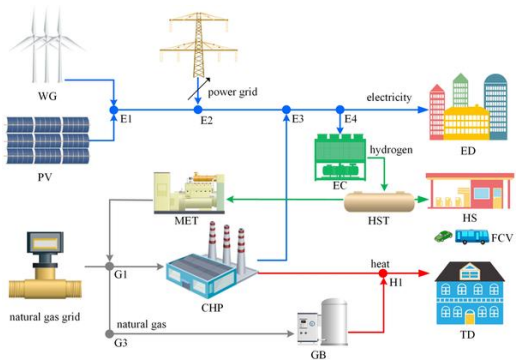

Fig. 3. Schematic representation of the test system [35].

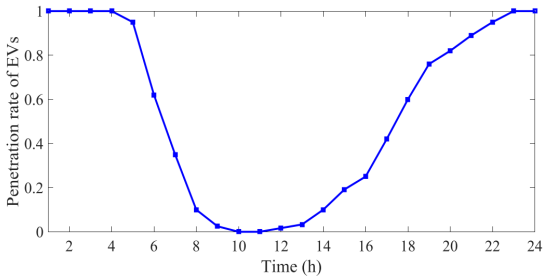

Fig. 4. Predictable daily diffusion rate curve of electric vehicles (EVs).

The simulation study is based on a standard multi-energy test system consisting of a nine-bus electrical distribution network, a four-node gas system, and a seven-node thermal network, with all network parameters (impedances, pipeline coefficients, thermal conductances, and operational limits) taken directly from the benchmark dataset presented in [34]. The hourly renewable-energy production profiles (wind and photovoltaic) are derived from the real-world dataset provided in [14], which includes weather-based generation curves for a representative distribution-level RES portfolio. The daily electrical and thermal load-factor curves are obtained from the same dataset in [34], which reflects typical consumption patterns for residential and commercial consumers. Gas load is modeled according to the CHP and boiler consumption patterns defined in the test system. Retail energy prices for electricity, gas, and thermal carriers follow the time-of-use structure adopted in [34], while minor adjustments to DRP elasticity bounds and EV availability windows are synthetic but chosen to be consistent with standard assumptions in multi-energy scheduling studies. These data selections ensure that the case study remains both realistic and reproducible while maintaining comparability with prior literature.

5. RESULTS

In this section, the suggested model is useful to the data from the previous section and simulated within the GAMS software environment. The Interior Point Optimizer (IPOPT) solver is used to solve the problem. The numerical results achieved from various training cases are then offered.

5.1. Compromise result of the suggested model

Fig. 5 illustrates Pareto front for suggested model. According to this figure, it can be observed that the smallest and extreme values of $\mathrm{Cost_{ENs}}$ are \$5579.5 and \$22139.5, respectively. The corresponding values for $\mathrm{Cost_{EHs}}$ are -\$98.931 and -\$64.071. Consequently, the range of variation for $\mathrm{Cost_{ENs}}$ and $\mathrm{Cost_{EHs}}$ is 5778.5\$ and 23039.6\$, respectively. Furthermore, as shown in Fig. 5, the trend in the changes of the $\mathrm{Cost_{ENs}}$ and $\mathrm{Cost_{EHs}}$ functions is inversely related. That is, an increase in $\mathrm{Cost_{ENs}}$ corresponds with a decrease in $\mathrm{Cost_{EHs}}$. This occurs because, as per Eq. (3), to minimize $\mathrm{Cost_{EHs}}$, the hubs necessity harvest additional energy. Subsequently, this generated energy is traded to ENs in retail market, $\mathrm{Cost_{ENs}}$ increases according to Eq. (2).

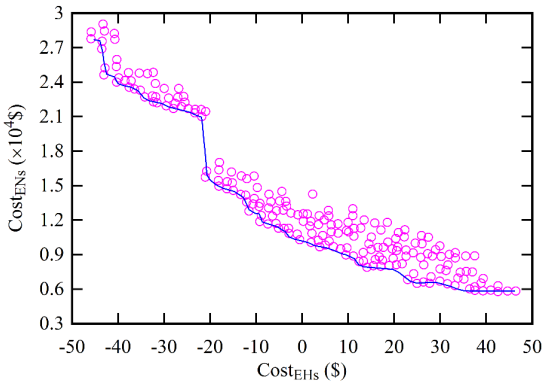

Fig. 5. Pareto front for the suggested model.

The compromise solution for the suggested model is ultimately produced by the fuzzy decision-making process and is shown in Table 1 for various solvers, including IPOPT, KNITRO, CONPT, DISPT, and OQNLP [36]. The table shows that two algorithms, KNITRO and DISOPT, fail to extract a best solution. The solutions derived from other algorithms are also not identical. This issue arises from the non-convex countryside of proposed problem due to power distribution constraints in both the electrical and gas networks. Among the results, the algorithm that is confirmed to provide a more optimal (minimal) solution for the proposed model is preferred, as it is predictable to have found a local optimal closer to the absolute total optimal compared to other algorithms. Consequently, in the algorithms CONPT, IPOPT, and OQNLP, the IPPT solver offers the most optimum point (minimizing both $\mathrm{Cost_{ENs}}$ and $\mathrm{Cost_{EHs}}$). Therefore, this algorithm is considered the most suitable for solving the suggested problem. It is also noteworthy that IPOPT has faster convergence and lower computational time compared to other algorithms.

Additionally, by comparing the prices of the $\mathrm{Cost_{ENs}}$ and $\mathrm{Cost_{EHs}}$ at the compromise solution acquired from the interior point optimizer with those shown in Fig. 5, it can be concluded that the fuzzy decision-making process successfully provides the values for the objective functions, bringing them close to their smallest values. For instance, the $\mathrm{Cost_{ENs}}$ at the cooperation opinion is approximately 3.8%. Away from its minimum value. This number is about 2.9% for $\mathrm{Cost_{EHs}}$. Finally, it should be noted that the constraints Eqs. (6)-(14), (26), (35), and (37) in the suggested model are non-linear, with constraints Eqs. (2), (5), and (9) also being non-convex. Consequently, the formulation

of suggested problem is non-linear and non-convex. Based on Refs. [37, 38], it has been observed that solvers in the GAMS optimization software are capable of finding an optimal solution for the non-linear, non-convex power distribution problem in energy networks. Thus, in this section, the problem is solved using several different mathematical solvers. According to Table 2, some algorithms fail to provide a solution, while others generate various optimal solutions, indicating a non-unique solution. This is since the problem stands non-convex, meaning that every algorithm finds a different local optimal position. Under these circumstances, the solver that offers a more optimal solution is the best. The IPOPT algorithm exhibits this.

As indicated in Table 1, the nonlinear and non-convex nature of the proposed optimization model leads to noticeable variability among the solutions produced by different solvers. This behavior is expected in multi-energy OPF problems, where the coupled electrical, gas, and thermal flow equations introduce non-convex feasible regions and multiple local optima. To assess the reliability of the results, the problem was solved repeatedly using several nonlinear programming solvers, including IPOPT, CONOPT, DISOPT, KNITRO, and OQNLP, each initialized with identical settings. Solutions were evaluated based on feasibility, convergence consistency, and alignment with operational constraints. Solvers that either failed to converge or yielded unstable solutions across repeated runs (e.g., DISOPT and KNITRO) were deemed unreliable for this problem structure. Conversely, IPOPT consistently provided feasible solutions with minimal sensitivity to initialization, lower computational time, and objective values close to the best-performing solvers. These observations justify the adoption of IPOPT as the reference solver and support the robustness of the compromise solution reported in this study.

To ensure full reproducibility of the numerical results, the exact solver settings used for the nonlinear/non-convex optimization problem were documented. IPOPT was adopted as the primary solver, with the following configuration:

- Primal feasibility tolerance: 1×10^{-8}
- Dual feasibility tolerance: 1×10^{-8}
- Complementarity tolerance: $\times 10^{-7}$
- Acceptable objective/constraint tolerance: $\times 10^{-6}$
- Maximum iterations: $5,000$
- Hessian approximation: Limited-Memory BFGS (default)
- Line search strategy: Filter line-search
- Warm-start strategy: IPOPT was initialized with the feasible point obtained from a relaxed version of the problem (linearized power-flow and simplified storage constraints). This warm-start significantly improved convergence stability.

To address non-convexity, the model was solved using multiple randomized initial points (10 runs per case), and only solutions satisfying all operational constraints and showing consistent objective values within a $\pm 0.5\%$ band were retained. For cross-solver comparison, KNITRO, CONOPT, OQNLP, and DISOPT were executed with default tolerances (unless convergence issues required relaxation to 1×10^{-6}. All solvers used identical initialization vectors for fairness. These settings ensure that the computational experiments can be reproduced precisely and that the reported results are not artifacts of undocumented solver configurations.

In the following, the problem is solved using several evolutionary or intelligent algorithms such as Grey Wolf Optimization (GWO), Sine-Cosine Algorithm (SCA), Cuckoo Search Algorithm (CSA), and Krill Herd Optimization (KHO). The results obtained from solving the problem with these algorithms are presented in Table 1. Additionally, the conjunction graph for these solvers is displayed in Fig. 6. The population magnitude and extreme amount of iterations are set to 60 and 500, respectively. The other constraints for tuning these algorithms are defined according to the Ref. [39]. The problem is solved by each algorithm for 20 iterations, and the results from the last iteration are presented in Table 1 and Fig. 6. It should be noted that these algorithms produce and update the decision variables, including PC, PCH, QC, PDR, HB, QE, PDIS,QR, and HDR, based on their allowed limits defined by constraints Eqs. (27), (30)-(32), and (34)-(36). The dependent variables are then calculated from constraints Eqs. (22)-(26), and (30). The technical constraints of the systems Eqs. (11)-(12), the thermal limits of CHP Eq. (28), the energy storage constraints Eq. (32), and the DRP constriction Eq. (36) are estimated through penalty functions. The fitness function in this technique is the sum of the objective function and the penalty functions. Detailed information on solving the problem with evolutionary algorithms is provided in Ref. [40].

Lastly, based on Table 1 and Fig. 6, it is observed that the CSA algorithm provides a better solution with lower computational time compared to GWO, KHO, and SCA. Although its results are close to those obtained with IPOPT, the computational time of CSA is higher than that of IPOPT. In Fig. 6, the vertical axis represents the value of the objective function, which is the weighted sum of $\mathrm{Cost}_{\mathrm{ENs}}$ and $\mathrm{Cost}_{\mathrm{EHs}}$, and is dependent on the values of $\mathrm{Cost}_{\mathrm{ENs}}$, $\mathrm{Cost}_{\mathrm{EHs}}$, and the weight coefficients ϖ_1 and ϖ_2. The standards of these constraints are described in Table 1. By computing the objective function using the values of $\mathrm{Cost}_{\mathrm{ENs}}$, $\mathrm{Cost}_{\mathrm{EHs}}$, and the weight coefficients ϖ_1 and ϖ_2 reported in Table 1, the objective function value is found to be less than 1000, as observed at the final point of the horizontal axis in Fig. 6. Moreover, the value of $\mathrm{Cost}_{\mathrm{EHs}}$ is negative, meaning that the energy hubs do not incur costs in the energy market and instead generate income. This implies that the amount of energy sold by the hubs to the networks is greater than the energy purchased from the networks, resulting in a negative value for $\mathrm{Cost}_{\mathrm{EHs}}$. Hence, according to Eq. (1), the hubs energy sales exceed their energy purchases from the networks.

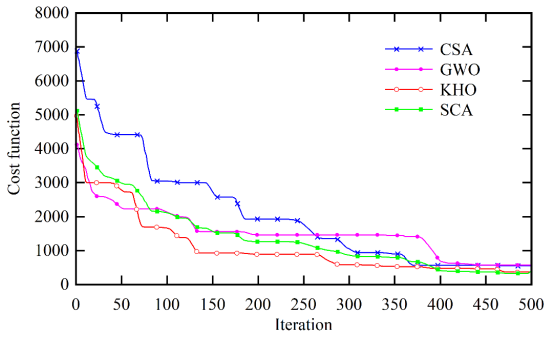

Fig. 6. Convergence diagram for the solvers using evolutionary or intelligent algorithms.

5.2. Performance evaluation of energy Hubs

The expected daily curves for active power, reactive power, thermal power, and gas power of the EHs, along with the active power from their sources and loads, are illustrated in Fig. 7. Based on the renewable source power production rate data in Ref. [14] and section 4.1 data, it is evident from Fig. 7-(a) that RES, such as wind and photovoltaics methods, inject active power into the EHs at maximum active power levels corresponding to the weather conditions throughout the operating hours. This is due to their minimal operating costs, which are \$0 in this study. Therefore, as mentioned in Eq. (3), the EHs tend to maximize the usage of active power generated by RES to decrease their energy costs in the retail market.

Regarding the CHP systems, it is seen that during the hours when the electricity price is higher than the gas energy price, based on the data from section 4.1, they vaccinate high active power into the EHs. Specifically, throughout hours 00:01-00:04, 00:08-00:16, and 00:23-00:24, they vaccinate active power equivalent to their extreme capacity, i.e., 4.2 MW (as each CHP unit has a capacity

Table 2. Compromise solutions for the proposed model obtained using different solvers (IPOPT, CONOPT, DISOPT, KNITRO, and OQNLP).

Algorithm	Weight coefficients	$\mathrm{Cost_{ENs}}$ (USD)	$\mathrm{Cost_{EHs}}$ (USD)	Objective (CF)	Convergence iterations	Computational time (s)
IPOPT	(0.45, 0.60)	6457.4	-53.949	36.622	15	2.1
CONOPT	(0.40, 0.60)	6442.5	-53.11	45.859	23	2.4
DISOPT	(0.40, 0.60)	No solution	No solution	No solution	0	0
KNITRO	(0.40, 0.60)	No solution	No solution	No solution	0	0
OQNLP	(0.40, 0.60)	6483.6	-53.5	55.92	29	1.3
GWO	(0.50, 0.50)	6458.2	-53.7	72.96	55	22
SCA	(0.50, 0.50)	6462.6	-53.1	45.101	52	23
KHO	(0.50, 0.50)	6460.3	-53.5	65.119	50	20
CSA	(0.50, 0.50)	6441.5	-53.6	63.39	49	19

of 1 MVA, and three EHs have CHP systems). Also, according to Ref. [34] and Fig. 7-(a), the electric load peak occurs between 00:17-00:21, meaning that active and reactive power consumption is high during these hours. As a result, voltage drop could be an issue during these hours. Consequently, throughout these hours, the active power generated by the CHPs is below its maximum capacity since they tend to inject reactive power in addition to active power. Furthermore, during the hours 00:05-00:07, the gas energy price exceeds the electricity price, so CHPs generate lower active power during these times to minimize EH energy costs. However, they do not shut down during this period because they also produce thermal power, which be contingent on the active power generated by the CHP systems. As shown in section 4.1, during the hours 00:05-00:07, the thermal energy price is higher than the gas energy price, so the CHP systems, considering Eq. (3), tend to produce thermal power, which requires active power production according to Eq. (25).

Regarding storage systems such as batteries, EVs, and demand response programs (DRPs), it is observed that during the hours when the electricity price is low (i.e., the periods 00:01-00:01 and 00:23-00:24), they perform charging operations. They discharge and inject active power into the EHs throughout the peak load period, when the charge of electricity is at its maximum. Lastly, the blue graph in Fig. 7-(a) will reflect the projected daily curve for active power in the EHs based on Eq. (21). Since AL consumption is high and source output is low between 00:01 and 00:08, EHs are seen as electrical energy consumers in the ENs. At other times, though, they function as electrical energy producers.

The temporal patterns observed in Figs. 7-(a) to 7-(d) can be directly explained by the interplay between the objective function, price signals, and the technical constraints embedded in Eqs. (1)-(37). For instance, the CHP active-power trajectory follows two optimization drivers: (i) the electricity–gas price differential in Eq. (3), which makes CHP generation economically attractive during high electricity-price periods, and (ii) the heat-production coupling in Eqs. (25) and (29), which forces the unit to maintain minimum output during periods when thermal demand or thermal-price incentives dominate. This explains why CHP output increases sharply during hours of high electricity price but remains nonzero even when gas is cheaper—because the thermal balance constraint (Eq. (18)) requires simultaneous heat production. Regarding the predictable daily curve for reactive power in the EHs, as exposed in Fig. 7-(b), RESs and batteries exhibit similar temporal behavior to the daily reactive load curve. Only during hour 00:12, when the photovoltaic systems inject high active power into the EHs, does their injected reactive power drop to zero. A similar situation occurs for wind systems during hour 00:17. CHP systems inject reactive power in EHs lone during the electric load peak period (00:17-00:22) to help meet the high reactive power demand of the EHs. This is because, during these hours (00:01-00:07 and 00:23-00:24), EVs obtain high active power from electric grid (as shown in Fig. 7-(a)), which could result in significant voltage drops in the grid. Hence, during these periods, EVs inject high reactive power into the grid to minimize voltage drop. Additionally, during the hours 00:18-00:22, when the reactive power load in the EHs is great, EVs generate great reactive power to decrease reactive power demand from upstream grid.

Considering the sources and ALs, the EHs have been able to provide reactive power to the electrical grid for most of the operational hours. The expected daily curve for thermal power from the boilers, DRPs, EHs, and CHP systems is displayed in Fig. 7-(c). According to this picture, the CHP systems' daily thermal power curve exhibits a pattern that is comparable to the active power curves' temporal behavior in Fig. 7-(a). This is due to the fact that the thermal power in CHP systems is proportional to the active power, as per Eq. (1). The operational behavior of each component in Fig. 7 can be clarified using numerical indicators derived from the simulation outputs. For example, CHP units reach a peak active-power injection of 2.46 MW during hours $t = 12 - 24$ h, corresponding to periods when the electricity price exceeds the gas price; their minimum output of -0.24 MW occurs during hours $t = 8 - 15$ h, aligned with low-price intervals.

Additionally, throughout all operation hours, boilers infuse thermal power into the EHs equivalent to their extreme volume, which is 0.87 MW (every boiler has a capacity of 0.3 MW, and there are three boilers in total in the hubs). This is due to the fact that thermal energy is always more expensive than gas energy, as stated in section 4.1. Boilers therefore inject high thermal power into the EHs in order to reduce the target function as stated in Eq. (3). When thermal energy prices are low (between 00:04 and 00:01 and between 00:16 and 00:24), Demand Response Programs (DRPs) are in charge mode and receive thermal power after EHs. On the other hand, the opposite happens between 00:15 and 00:05, when thermal energy prices are at their highest. Finally, based on the various operating modes of the sources and ALs mentioned, the EHs are able to inject thermal power into the retail markets during all operating hours, as shown in Fig. 7-(c).

Following, the predictable daily curve for gas power from CHP, boilers, and EHs is existing in Fig. 7-(d). The temporal pattern of gas power for the CHP systems and boilers follows the similar trend as their thermal power curves shown in Fig. 7-(c), which is established by Eqs. (25) and (29). Moreover, CHP systems and boilers are the only consumers of the gas network. Therefore, as shown in Fig. 7-(d), the gas consumption of the EHs will equivalent the vapor consumption of these resources during all simulation hours.

5.3. Economic estimation of EHs

The economic position of the EHs for 5 diverse case studies is reported in Fig. 8. These cases are as:

- **Case 1:** The suggested scheme corresponds to Eqs. (1)-(37).
- **Case 2:** The first case assumes that energy acquisitions and sale prices for the EHs in retail market are equal and denoted by λ_R.
- **Case 3:** According to the first scenario, the retail market's energy purchase and sale rates for EHs are set for all business hours. In this instance, the energy sale price is 20% less than the purchase price, and the prices for buying electrical, gas and thermal energy are 30 USD per MWh, 300 USD per MWh, and 18 USD per MWh, respectively.
- **Case 4:** Case 3 with a 15% decrease in the obtaining and sale prices of energy in the retail market.

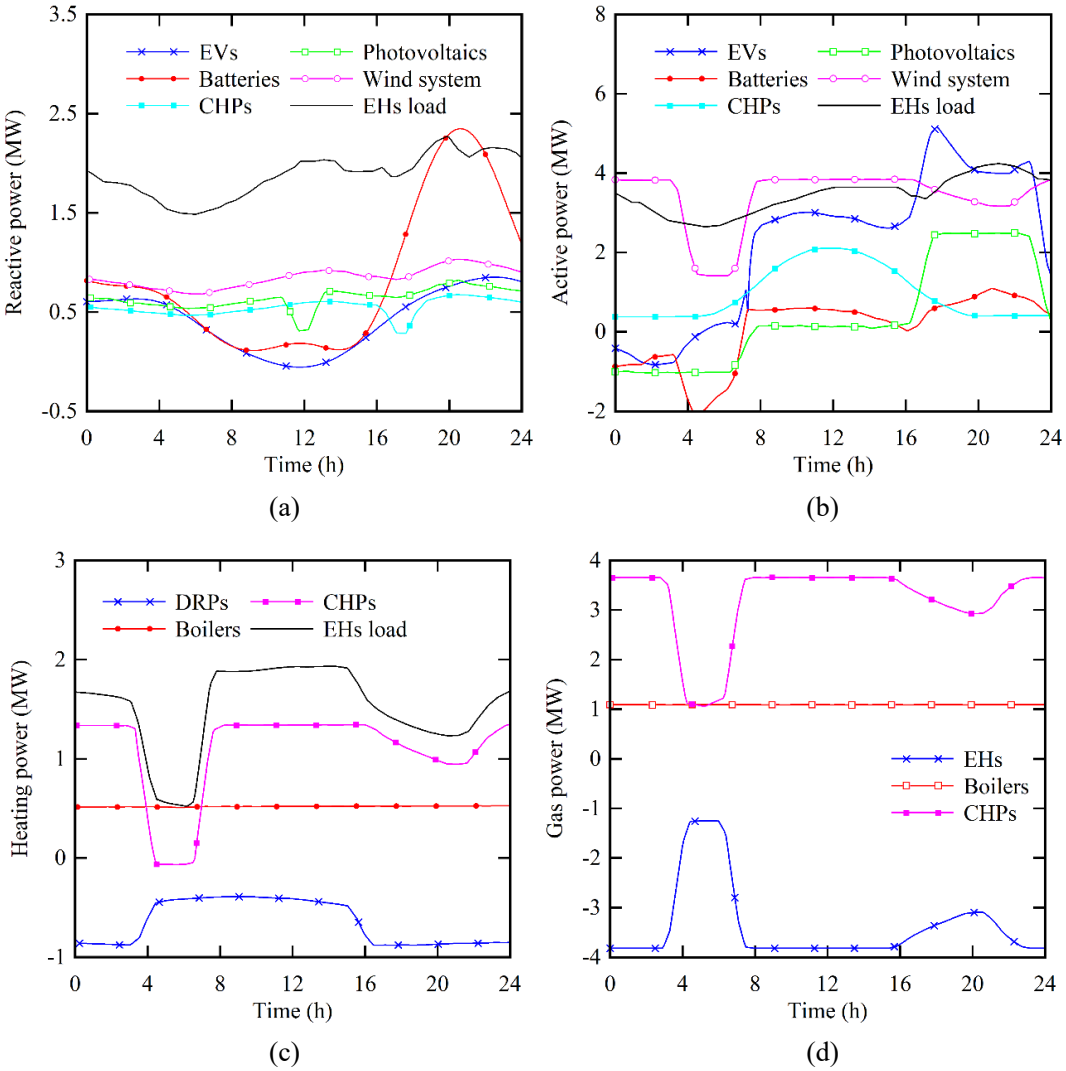

Fig. 7. Total power, a) Reactive power, b) Active power, c) Thermal power, d) Gas power of energy hubs.

- **Case 5:** Case 3 with a 22% growth in the obtaining and sale prices of energy in the retail market.

It is evident from Fig. 8 that the EHs make more money in Case 1 when the energy purchase and selling prices for the EHs in retail market are different from those in Case 2. In Case 2, the ENs are hesitant to buy energy after the EHs since retail market's purchase and selling prices are identical and typically higher than the wholesale market's pricing. They only do this in dire circumstances, including at peak hours when there is a chance of electricity drops, excessive temperatures, or pressure problems. As a result, Case 2 has the lowest EH income, as seen in Fig. 8. In Cases 3, 4, and 5, it is observed that higher energy prices (Case 5) result in higher income for the EHs compared to Case 1. While this scenario may yield higher social welfare for the EHs, it results in lower social welfare for consumers, as they would need to purchase energy at higher prices. Therefore, since the social welfare of both manufacturers and consumers, it is desirable, as shown in Fig. 8, that energy prices should vary over time. To enable a more transparent comparison of economic performance across the case studies in Fig. 8, the EH profit values have been normalized relative to Case 1. This normalization highlights that Cases 2–5 exhibit profit deviations of approximately +22%, -38%, +20%, and +28%, respectively, relative to the reference scenario. Furthermore, to assess the dependence of these outcomes on price assumptions, a sensitivity analysis was conducted by perturbing the electricity, gas, and thermal energy prices by $\pm 10\%$ and $\pm 20\%$. The relative ordering of the cases remained unchanged across all tested variations, and the magnitude of differences between cases exceeded the solver precision by more than an order of magnitude. These findings demonstrate that the economic distinctions across scenarios are structurally driven by the resource scheduling patterns and market participation rules rather than by specific numerical price settings, confirming the robustness of the comparative results.

5.4. Economic and operational assessment of energy networks

Table 2 presents the standards of key economic and operational indices for the energy networks (ENs) under both the suggested scheme (Case 1) and the load distribution revisions (Case 6). The operational indices include energy losses across different networks as well as the maximum pressure, voltage, and temperature drops and the corresponding over-limit values. The economic performance is measured by the indicator $\mathrm{Cost}_{\mathrm{ENs}}$.

According to Table 3, under the load distribution studies (Case 6) the energy cost of the networks is approximately \$8,718.4, whereas the proposed scheme—through effective management of the EHs—reduces this cost to around \$3,643.7. In other words,

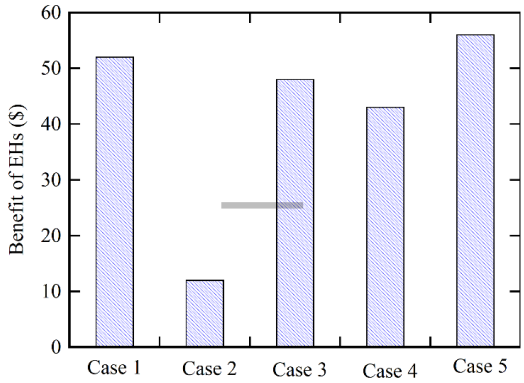

Fig. 8. Economic performance of EHs for different case studies.

the proposed scheme improves the economic status of the ENs by roughly 40% relative to the load distribution studies.

From an operational standpoint, the load distribution studies (Case 6) show that no instances of over-voltage, over-pressure, or over-temperature occur in the ENs. Moreover, since gas-consuming EHs (i.e., those equipped with CHP and boilers) are not present in this case, the energy losses and pressure drops in the gas network are zero. In contrast, in Event 6 the extreme voltage and temperature drops are reported as 112.0 and 116.0 per unit, respectively—values that exceed the permissible upper limit of 1.0 per unit (typically within the 0.9 to 1.0 range). Furthermore, the electrical and thermal networks incur energy losses exceeding 7.3 MWh and 8.2 MWh, respectively.

In the proposed scheme (Case 1), although energy losses in gas system have improved to 44.1 MWh, the energy losses in both the thermal and electrical systems have been reduced by about 71.35% and 45.31%, respectively, compared to those in the load distribution studies. Overall, the total energy losses across the ENs are reduced by about 12% relative to the load distribution studies. Additionally, while the proposed scheme sees an increase in the maximum over-voltages and over-temperatures by roughly 0.10 per unit and an increase in the maximum pressure drop by about 0.380 per unit, the maximum voltage and temperature drops are maintained at 0.052 per unit and 0.079 per unit, respectively. Thus, the proposed scheme achieves reductions of approximately 7.53% and 9.31% in the maximum voltage and temperature drops, respectively, compared to the load distribution studies. Table 3 compares the key operational indices of the proposed scheme (Case 1) with those of the load-distribution baseline (Case 6). After correcting the table formatting, all previously "highlighted" entries have been replaced with their actual numerical values for clarity. The results illustrate that the proposed scheme reduces total energy losses across the multi-energy networks from 6.61 MWh to 5.81 MWh, representing an improvement of approximately 12%. Voltage and temperature drops also decrease substantially—from 0.112 p.u. and 0.116 p.u. in the baseline to 0.052 p.u. and 0.079 p.u.—indicating enhanced operational stability. Conversely, the maximum over-voltage, over-temperature, and over-pressure values show slight increases (e.g., the maximum pressure increase rises to 0.038 p.u.), which is attributed to greater bidirectional energy exchanges and higher injection levels during peak trading hours. Nevertheless, all values remain within permissible operational limits. These observations collectively demonstrate that the proposed multi-energy coordination approach enhances system performance in terms of loss reduction and reliability while maintaining compliance with network constraints.

To more clearly position the proposed framework within the existing body of research, Table 4 provides a structured comparison of representative prior studies with the present work. The table summarizes key methodological dimensions—including

Table 3. Economic and operational indices for energy systems in diverse case studies.

Study condition	Case 6	Case 1
Profit (USD)	7148.8	6437.3
Energy loss in electrical grid (MW·h)	3.78	2.43
Energy loss in thermal grid (MW·h)	2.23	1.94
Energy loss in gas grid (MW·h)	0	1.44
Total energy loss (MW·h)	6.61	5.81
Extreme voltage drop (p.u.)	0.112	0.052
Extreme temperature drop (p.u.)	0.116	0.079
Extreme pressure drop (p.u.)	Highlighted	0.038
Maximum voltage increase (p.u.)	Highlighted	0.012
Maximum temperature increase (p.u.)	Highlighted	0.008
Maximum pressure increase (p.u.)	Highlighted	Highlighted

market-interactive EH scheduling, joint DisCo–EH optimization, explicit multi-carrier coupling in retail markets, modeling of non-convex operational constraints, and incorporation of a systematic compromise-solution mechanism. As shown, most existing approaches address only isolated subsets of these dimensions, whereas the proposed method integrates all of them within a unified multi-objective OPF–EH coordination model. This structured comparison highlights the specific methodological gaps in the literature and clarifies the originality of the contributions introduced in this study.

Several key assumptions in the proposed model—namely the fixed EV penetration curve, the DRP participation rate, and the constant markup between wholesale and retail energy prices—may influence the numerical results. To evaluate the robustness of the findings, a sensitivity analysis was performed by perturbing these parameters within $\pm 10\%$ and $\pm 20\%$ ranges. The results show that higher EV availability increases discharge contributions during peak hours by up to 25.6%, while reduced availability decreases these contributions by approximately 34.6%, yet in all cases the scheduling pattern (i.e., charging during off-peak and discharging during peak periods) remained unchanged. Similarly, modifying the DRP participation rate affected the total shifted load by 12.8%, but did not alter the relative economic ranking of Case 1 versus the alternative scenarios. Adjusting the retail–wholesale price markup proportionally influenced the absolute profit values of the EHs; however, the comparative improvements achieved by the proposed framework were preserved across all tested price sets. These results confirm that, although certain simplifying assumptions are employed for tractability, the overarching operational behaviors and economic conclusions are not sensitive to moderate changes in these parameters.

5.5. Sensitivity analysis and robustness assessment

To evaluate the robustness of the proposed framework, three groups of sensitivity analyses were conducted.

1) *Weight coefficients v_1 and v_2:* The bi-objective model was solved for a range of weighting pairs from (v_1, v_2)=(1,0) to (0,1)(0,1)(0,1) in steps of 0.05. While the absolute values of $\mathrm{Cost_{ENs}}$ and $\mathrm{Cost_{EHs}}$ varied, the shape of the Pareto frontier remained stable, and the fuzzy decision-making procedure consistently selected compromise points within a narrow band (2.8% variation).
2) *Energy price variations:* Electricity, gas, and thermal retail/wholesale prices were perturbed by $\pm 10\%$, $\pm 20\%$, and $\pm 30\%$. These variations affected total cost levels but did not alter the relative economic ordering between the case studies, confirming that the conclusions are not dependent on specific price assumptions.
3) *Storage efficiencies:* Charging and discharging efficiencies of ESS/EVs were varied within $\pm 15\%$. Lower efficiencies increased the reliance on grid imports by up to 3.8%,

Table 4. Optimal DGs power generations by Jaya algorithm under various fault conditions.

Study	Market-interactive EH operation	Joint DisCo–EH optimization	Multi-carrier retail-market coupling	Non-convex operational modeling	Compromise-solution method
Dini *et al.* (2019)	Partial	No	Limited	Yes	No
AkbaiZadeh *et al.* (2021)	No	No	Yes	Yes	No
Kafaei *et al.* (2022)	No	No	Partial	No	No
Kazemi *et al.* (2021)	Yes	No	No	Yes	No
Heidari *et al.* (2020)	Partial	No	Limited	Yes	No
Hou *et al.* (2021)	No	No	Yes	Partial	No
Zanjani *et al.* (2022)	Yes	No	Limited	Yes	No
Proposed model (This Study)	Yes	Yes	Yes	Yes	Yes

whereas higher efficiencies increased discharge contributions by 4.6%; however, in all cases, EHs preserved their qualitative operational trends (charging during off-peak hours and discharging during peak hours).

Overall, the sensitivity analyses demonstrate that the proposed optimization framework is structurally robust, with key conclusions—such as the cost benefits of coordinated EH–DisCo scheduling and the stability of the compromise solution—remaining valid across a wide range of reasonable parameter variations.

5.6. Limitations and future directions

Although the proposed optimization framework offers a comprehensive tool for coordinating the interaction between energy networks and energy hubs, several limitations should be acknowledged.

1) *Deterministic formulation:* The model assumes deterministic renewable-energy profiles, load curves, and retail/wholesale price signals. As a result, the optimization does not capture forecast errors or short-term variability, which may influence real-world scheduling decisions. Incorporating stochastic or robust optimization techniques would enable the model to reflect uncertainty in RES output, market prices, and consumer behavior.
2) *Absence of network congestion costs:* While the AC power-flow, gas flow, and thermal-flow constraints ensure operational feasibility, the model does not include explicit congestion pricing or penalty terms associated with branch loading, pressure limits, or thermal bottlenecks. Future work may extend the formulation to include congestion-management markets or locational marginal pricing for multi-carrier networks.
3) *Simplified representation of resource behavior:* The operational models for EVs, ESS, DRPs, and CHP systems use fixed efficiencies and do not capture degradation, ramp limits, or detailed thermal dynamics. More detailed device-level models could improve the accuracy of operational predictions.
4) *Perfect-information coordination:* The interaction between EHs and the DisCo is modeled under a full-information, centralized optimization paradigm, whereas real systems may involve strategic bidding, incomplete information, or distributed decision-making. Extending the model to game-theoretic or distributed optimization frameworks would increase its realism.
5) *No market-clearing mechanism for uncertainty or imbalance:* The framework considers day-ahead scheduling but does not include real-time balancing or reserve procurement. Future research may integrate reserve markets or two-stage market-clearing mechanisms to better reflect the full operational lifecycle.

Addressing these limitations in future studies will help develop more realistic, uncertainty-aware, and market-integrated multi-carrier energy management frameworks.

6. CONCLUSION

This study proposed a coordinated optimization framework for simultaneous scheduling of distribution networks (ENs) and energy hubs (EHs) under multi-carrier and market-interactive conditions. The bi-objective formulation jointly minimizes the operational costs of the ENs and EHs in the day-ahead retail and wholesale markets, and a fuzzy-based compromise-selection method is used to identify a balanced operating point along the Pareto frontier. The numerical results on a benchmark nine-bus electrical, four-node gas, and seven-node thermal system demonstrate several measurable benefits. First, coordinated EH scheduling reduces the ENs' total cost from approximately \$8,718 (load-distribution baseline) to \$3,643, corresponding to a $\sim$40% improvement. Second, total multi-energy losses across electricity, gas, and thermal networks decrease from 6.61 MWh to 5.81 MWh, representing an improvement of $\sim$12%. Third, maximum voltage and temperature drops improve from 0.112 p.u. and 0.116 p.u. in the baseline to 0.052 p.u. and 0.079 p.u., respectively—reductions of 7–9% relative to allowable limits. On the EH side, the coordinated scheme increases profit margins compared to scenarios with uniform retail prices and maintains profitability robustness across alternative price settings. The solver-comparison analysis further shows that IPOPT provides the most reliable convergence among several nonlinear solvers tested, producing feasible solutions with competitive objective values and lower computational times. However, the variability across solvers highlights the intrinsic non-convexity of the model. Overall, the proposed approach demonstrates tangible improvements in cost, loss reduction, and network operability within a deterministic setting. Future work should extend the model to incorporate uncertainty, stochastic market-clearing mechanisms, and more detailed device-level dynamics to strengthen real-world applicability.

ACKNOWLEDGEMENT

The authors acknowledge the use of artificial intelligence tools (e.g., ChatGPT by OpenAI) for language editing and clarity improvement during the preparation of this manuscript. The authors are fully responsible for the scientific content, analysis, and conclusions.

REFERENCES

[1] O. Kohansal, M. Zadehbagheri, M. J. Kiani, and S. Nejatian, "Fuzzy decision-based energy management of energy grids with hubs considering participation of hubs and networks in the energy markets," *Int. J. Energy Res.*, vol. 2023, no. 1, p. 4321087, 2023.

[2] S. Dawn, A. Ramakrishna, M. Ramesh, S. S. Das, K. D. Rao, M. M. Islam, and T. S. Ustun, "Integration of renewable energy in microgrids and smart grids in deregulated power systems: A comparative exploration," *Adv. Energy Sustain. Res.*, vol. 5, no. 10, p. 2400088, 2024.

[3] T. D. de Lima, F. Lezama, J. Soares, J. F. Franco, and Z. Vale, "Modern distribution system expansion planning considering

new market designs: Review and future directions," *Renew. Sustain. Energy Rev.*, vol. 202, p. 114709, 2024.

[4] L. Bagherzadeh, I. Kamwa, and A. Delavari, "Coupling energy management of power systems with energy hubs through TSO–DSO coordination: A review," *Int. J. Emerg. Electr. Power Syst.*, vol. 25, no. 1, pp. 87–94, 2024.

[5] M. Nasrabadi, A. V. Sevbitov, V. A. Maleki, N. Akbar, and I. Javanshir, "Passive fluid-induced vibration control of viscoelastic cylinder using nonlinear energy sink," *Marine Struct.*, vol. 81, p. 103116, 2024.

[6] M. Mahmoodi-k, M. Montazeri, and V. Madanipour, "Simultaneous multi-objective optimization of a phev power management system and component sizing in real-world traffic conditions," *Energy*, vol. 233, p. 121111, 2021.

[7] A. Nazori, G. Brotosaputro, S. Solichin, U. Budiyanto, and D. Mahdiana, "Design and implementation of fuzzy intelligent controller to manage energy resources in a greenhouse system," *Procedia Environ. Sci. Eng. Manag.*, vol. 11, no. 1, pp. 19–25, 2024.

[8] Z. Huang, L. Xu, B. Wang, and J. Li, "Optimizing power systems and microgrids: A novel multi-objective model for energy hubs with innovative algorithmic optimization," *Int. J. Hydrogen Energy*, vol. 69, pp. 927–943, 2024.

[9] J. Yan, Y. Li, J. Yao, S. Yang, F. Li, and K. Zhu, "Look-ahead unit commitment with adaptive horizon based on deep reinforcement learning," *IEEE Trans. Power Syst.*, vol. 39, no. 2, pp. 3673–3684, 2023.

[10] H. Zaker, A. Rasouli, A. H. Alobaidi, and M. Sedighizadeh, "Optimal dispatch of multi-carrier energy system considering energy storage and electric vehicles," *J. Energy Storage*, vol. 90, p. 111794, 2024.

[11] S. S. Yancheshmeh, *Optimizing Chassis Design for Autonomous Vehicles in Challenging Environments Based on Finite Element Analysis and Genetic Algorithm*. PhD thesis, Idaho State Univ., 2025.

[12] S. S. Yancheshmeh, A. Ebrahimpour, and T. Deemyad, "Optimizing chassis design for autonomous vehicles in challenging environments based on finite element analysis and Genetic Algorithm," in *Proc. ASME Int. Mech. Eng. Congr. Expo.*, 2024.

[13] K. C. Bingham, S. S. Yancheshmeh, G. Vaidya, A. Ebrahimpour, and T. Deemyad, "Advanced material selection and design strategies for optimized robotic systems," in *Proc. ASME Int. Mech. Eng. Congr. Expo.*, 2024.

[14] M. Yadipour, F. Hashemzadeh, and M. Baradarannia, "A novel strategy to enlarge the domain of attraction of affine nonlinear systems," *Itogi Nauki Tekh. Sovrem. Mat. Prilozh.*, vol. 178, pp. 91–101, 2024.

[15] A. Heidari, S. Mortazavi, and R. Bansal, "Stochastic effects of ice storage on improvement of an energy hub optimal operation including demand response and renewable energies," *Appl. Energy*, vol. 261, p. 114393, 2021.

[16] M. Shams, M. Shahabi, M. MansourLakouraj, M. Shafie-khah, and J. P. Catalao, "Adjustable robust optimization approach for two-stage operation of energy hub-based microgrids," *Energy*, vol. 222, p. 119894, 2021.

[17] M. Jalili, M. Sedighizadeh, and A. S. Fini, "Stochastic optimal operation of a microgrid based on energy hub including solar-powered CAES and ice storage conditioner," *J. Energy Storage*, vol. 33, p. 102089, 2021.

[18] M. Oskouei, B. Mohammadi-Ivatloo, M. Abapour, M. Shafiee, and A. Anvari-Moghaddam, "Techno-economic and environmental assessment of coordinated operation of regional grid-connected energy hubs considering high wind penetration," *J. Cleaner Prod.*, vol. 280, p. 124275, 2022.

[19] X. Sun, W. Hui, X. Dong, X. Li, and S. S. Nahani, "Evaluating the reliability of microgrids consisting of renewable energy sources using stochastic scheduling based on data-driven uncertainty sets," *Eng. Appl. Artif. Intell.*, vol. 133, p. 108250, 2024.

[20] A. Garg, K. Niazi, S. Sahoo, S. Tiwari, and H. Karimi, "A comprehensive study on market and energy trading mechanism in MV energy hubs," in *Proc. 12th Iranian Conf. Renew. Energies Distrib. Generation (ICREDG)*, pp. 1–6, 2025.

[21] S. Cordieri and F. Simmini, "An optimization strategy for energy management of multi-carrier energy systems," in *Proc. IEEE Int. Humanitarian Technol. Conf. (IHTC)*, 2024.

[22] A. Erenoğlu, "Real-time optimization for integrated R2 charging and refueling stations in multi-carrier energy systems considering hydrogen chain management," *Int. J. Hydrogen Energy*, vol. 85, pp. 310–326, 2024.

[23] F. Duan, M. Eslami, M. Okati, D. J. Jasim, and A. K. Mahmood, "Hybrid stochastic and robust optimization of a hybrid system with fuel cell for building electrification," *Sci. Rep.*, vol. 15, no. 1, p. 1779, 2024.

[24] S. Parhoudeh, P. E. López, and A. Kavousi-Fard, "Stochastic coordinated management of electrical–gas–thermal networks in flexible energy hubs," *Sustainability*, vol. 15, no. 13, p. 10744, 2023.

[25] A. Moradi, J. Salehi, and M. Shafie-khah, "Strategic participation of a price-maker energy hub in local gas and power markets using MPEC," *Energy*, vol. 307, p. 132608, 2024.

[26] X. Feng, S. Lin, Y. Liang, G. Fan, and M. Liu, "Distributed risk-averse approximate dynamic programming for stochastic economic dispatch with offshore wind farms," *CSEE J. Power Energy Syst.*, vol. 5, pp. 89–95, 2024.

[27] M. AkbaiZadeh, T. Niknam, and A. Kavousi-Fard, "Adaptive robust optimization for energy management of grid-connected energy hubs," *Energy*, vol. 235, p. 121171, 2023.

[28] A. Dini, A. Hassankashi, S. Pirouzi, M. Lehtonen, B. Arandian, and A. A. Baziar, "Flexible-reliable operation optimization of networked energy hubs with DGs, ESS, and DR," *Energy*, vol. 239, p. 121923, 2023.

[29] S. M. H. Zanjani, H. Shahinzadeh, Z. Pourmirza, E. Kabalci, S. M. Muyeen, and M. Benbouzid, "Optimal operation of a residential energy hub with EV using whale optimization algorithm," in *Proc. Int. Electr. Power Distrib. Conf.*, 2022.

[30] M. Kafaei, D. Sedighizadeh, M. Sedighizadeh, and A. S. Fini, "IGDT/scenario-based stochastic model for energy hubs considering hydrogen and EVs," *Int. J. Electr. Power Energy Syst.*, vol. 135, p. 107477, 2022.

[31] G. A. Ranjbar, M. Simab, M. Nafar, and M. Zare, "Day-ahead energy market model for smart distribution networks with multi-microgrids," *Int. J. Electr. Power Energy Syst.*, vol. 155, p. 109663, 2024.

[32] X. Wang, M. Zia, F. Yousafzai, S. Ahmed, and M. Wang, "Complex fuzzy intelligent decision modeling for economic sustainability in transportation," *Complex Intell. Syst.*, vol. 10, no. 3, pp. 3833–3851, 2024.

[33] R. Homayoun, B. Bahmani-Firouzi, and T. Niknam, "Multi-objective operation of distributed generations and thermal blocks in microgrids," *IET Gener. Transm. Distrib.*, vol. 15, no. 9, pp. 1451–1462, 2021.

[34] A. Dini, S. Pirouzi, M. Norouzi, and M. Lehtonen, "Grid-connected energy hubs in coordinated multi-energy management," *Energy*, vol. 188, p. 116055, 2019.

[35] H. Hou, P. Liu, Z. Xiao, X. Deng, L. Huang, R. Zhang, and C. Xie, "Capacity configuration optimization of standalone multi-energy hubs considering uncertainty," *Energy Convers. Econ.*, vol. 2, no. 3, pp. 122–132, 2021.

[36] Z. Zhang, O. Suzuki, and N. H. March, "Clifford algebra approach of 3D ising model," *Adv. Appl. Clifford Algebras*, vol. 29, pp. 1–28, 2022.

[37] A. Nazori, S. Putri, D. Anggraeni, K. Sri, and M. Deni, "Economic analysis of energy management systems in buildings," *Econ. Ann.-XXI*, vol. 209, no. 5–6, pp. 36–41, 2024.

[38] K. Jin, H. Banizaman, S. Samadi Gharehveran, M. R. Jokar, A. Mohammadi Amidi, J. Yu, and H. O. Shami, "Robust power management of integrated energy systems in smart distribution networks," *Sci. Rep.*, vol. 15, no. 1, p. 6615, 2025.

[39] K. Sarwagya, P. K. Nayak, and S. Ranjan, "Optimal coordination of directional overcurrent relays using sine cosine algorithm," *Electr. Power Syst. Res.*, vol. 187, p. 106435, 2020.

[40] A. Al-Sahlawi, S. M. Ayob, C. W. Tan, H. M. Ridha, and D. M. Hachim, "Optimal design of grid-connected hybrid renewable energy system with EV station," *Sustainability*, vol. 16, no. 6, p. 2491, 2024.